JOURNAL OF GEOPHYSICAL RESEARCH, VOL. 109, C08S02, doi:10.1029/2003JC002256, 2004

Air-sea CO_2 exchange in the equatorial Pacific

Wade R. McGillis,[1,2] James B. Edson,[3] Christopher J. Zappa,[1] Jonathan D. Ware,[3] Sean P. McKenna,[3] Eugene A. Terray,[3] Jeffrey E. Hare,[4,5] Christopher W. Fairall,[6] William Drennan,[7] Mark Donelan,[7] Michael D. DeGrandpre,[8] Rik Wanninkhof,[9] and Richard A. Feely[10]

Received 17 December 2003; revised 7 July 2004; accepted 21 July 2004; published 28 August 2004.

[1] GasEx-2001, a 15-day air-sea carbon dioxide (CO_2) exchange study conducted in the equatorial Pacific, used a combination of ships, buoys, and drifters equipped with ocean and atmospheric sensors to assess variability and surface mechanisms controlling air-sea CO_2 fluxes. Direct covariance and profile method air-sea CO_2 fluxes were measured together with the surface ocean and marine boundary layer processes. The study took place in February 2001 near 125°W, 3°S in a region of high CO_2. The diurnal variation in the air-sea CO_2 difference was 2.5%, driven predominantly by temperature effects on surface solubility. The wind speed was 6.0 ± 1.3 m s^{-1}, and the atmospheric boundary layer was unstable with conditions over the range $-1 < z/L < 0$. Diurnal heat fluxes generated daytime surface ocean stratification and subsequent large nighttime buoyancy fluxes. The average CO_2 flux from the ocean to the atmosphere was determined to be 3.9 mol m^{-2} yr^{-1}, with nighttime CO_2 fluxes increasing by 40% over daytime values because of a strong nighttime increase in (vertical) convective velocities. The 15 days of air-sea flux measurements taken during GasEx-2001 demonstrate some of the systematic environmental trends of the eastern equatorial Pacific Ocean. The fact that other physical processes, in addition to wind, were observed to control the rate of CO_2 transfer from the ocean to the atmosphere indicates that these processes need to be taken into account in local and global biogeochemical models. These local processes can vary on regional and global scales. The GasEx-2001 results show a weak wind dependence but a strong variability in processes governed by the diurnal heating cycle. This implies that any changes in the incident radiation, including atmospheric cloud dynamics, phytoplankton biomass, and surface ocean stratification may have significant feedbacks on the amount and variability of air-sea gas exchange. This is in sharp contrast with previous field studies of air-sea gas exchange, which showed that wind was the dominating forcing function. The results suggest that gas transfer parameterizations that rely solely on wind will be insufficient for regions with low to intermediate winds and strong insolation. *INDEX TERMS:* 0312 Atmospheric Composition and Structure: Air/sea constituent fluxes (3339, 4504); 3307 Meteorology and Atmospheric Dynamics: Boundary layer processes; 3339 Meteorology and Atmospheric Dynamics: Ocean/atmosphere interactions (0312, 4504); 4231 Oceanography: General: Equatorial oceanography; 4227 Oceanography: General: Diurnal, seasonal, and annual cycles; *KEYWORDS:* air-sea carbon dioxide fluxes, equatorial Pacific, direct covariance technique, profile flux technique, diurnal surface layer

Citation: McGillis, W. R., et al. (2004), Air-sea CO_2 exchange in the equatorial Pacific, *J. Geophys. Res.*, *109*, C08S02, doi:10.1029/2003JC002256.

1. Introduction

[2] Processes near the air-water interface of the ocean surface play an important role in the exchange of CO_2 to and from the atmosphere. Despite this, some fundamental

[1]Lamont-Doherty Earth Observatory, Palisades, New York, USA.
[2]Also at Department of Earth and Environmental Engineering, Columbia University, New York, USA.
[3]Woods Hole Oceanographic Institution, Woods Hole, Massachusetts, USA.
[4]Cooperative Institute for Research in Environmental Sciences, University of Colorado, Boulder, Colorado, USA.
[5]Also at NOAA Environmental Technology Laboratory, Boulder, Colorado, USA.
[6]NOAA Environmental Technology Laboratory, Boulder, Colorado, USA.
[7]Division of Applied Marine Physics, Rosenstiel School of Marine and Atmospheric Science, University of Miami, Miami, Florida, USA.
[8]Department of Chemistry, University of Montana, Missoula, Montana, USA.
[9]NOAA Atlantic Oceanographic and Meteorological Laboratory, Miami, Florida, USA.
[10]NOAA Pacific Marine and Environmental Laboratory, Seattle, Washington, USA.

0148-0227/04/2003JC002256$09.00

mechanisms that control the rate of transfer have not been well resolved. While globally the ocean absorbs a significant amount of atmospheric carbon, regionally the ocean has strong local sinks and sources. The CO_2 that is exchanged between the ocean and atmosphere is not highly soluble in water. Thus molecular diffusion and turbulent mixing at the aqueous boundary layer are the important transport processes controlling the CO_2 exchange rate across the surface. The aqueous boundary layer and the corresponding CO_2 exchange rate are affected by local meteorological and environmental conditions in both the atmosphere and ocean. To quantify the ocean-atmosphere exchange, CO_2 transport through the marine atmospheric boundary layer was measured during GasEx-2001 using various micrometeorological techniques and heat proxies [*Garbe et al.*, 2004].

[3] Aside from CO_2, exchange of climate relevant compounds such as DMS, CO_2 fluorocarbons, and methane across the air-sea interface is of central interest. Understanding the processes that control air-sea exchange and assessing the magnitude of air-sea fluxes are high-priority objectives of climate researchers. This information will enable physically based, ocean biogeochemical models to more accurately estimate regional and global fluxes and to predict the feedback between air-sea gas exchange and climate.

[4] While progress has been made in studying gas exchange [*Broecker and Peng*, 1974; *Smith and Jones*, 1985; *Broecker et al.*, 1986; *Asher and Wanninkhof*, 1998; *Donelan and Drennan*, 1995; *Jähne and Haussecker*, 1998; *Jacobs et al.*, 1999; *Bock et al.*, 1999; *Nightingale et al.*, 2000; *McGillis et al.*, 2001a, 2001b; *Zemmelink et al.*, 2004; *Wanninkhof et al.*, 2004], an adequate understanding of the fundamental physical processes or an ability to accurately infer gas exchange rates from remotely observable properties of the sea surface does not exist. One of the major challenges of research in this area is the simultaneous measurement of the wide range of parameters needed to characterize turbulent exchange across the air-sea interface.

[5] Several advances in micrometeorological techniques address the concerns related to oceanic applications [*Fairall et al.*, 2000]. Advances in atmospheric profile and covariance methods have decreased the timescale for flux measurement to subhour. This is particularly true for the ocean-atmosphere direct covariance method for CO_2 [*Donelan and Drennan*, 1995; *McGillis et al.*, 2001a], the profile method [*Dacey et al.*, 1999; *McGillis et al.*, 2001b; *Zemmelink et al.*, 2004], and direct covariance for dimethylsulfide (DMS) [*Mitchell*, 2001]. Short time frame flux measurements permit the analysis of processes that regulate gas exchange and also increase statistical confidence in examining these relationships. However, problematic issues for air-sea gas flux measurements by micrometeorological techniques include: (1) degradation of the measurements from motions of mobile platforms such as ships and aircraft, (2) errors from flow distortion around the measurement platform, and (3) inadequate gas sensor sensitivity and frequency response.

[6] GasEx-2001 was an equatorial Pacific air-sea CO_2 process study conducted to quantify the regional CO_2 flux and the controlling physical and biogeochemical processes [see *Johnson et al.*, 2004; *Feely et al.*, 2004; *Sabine et al.*, 2004; *Ward et al.*, 2004; *DeGrandpre et al.*, 2004; *Strutton et al.*, 2004]. Simultaneous micrometeorological gas flux and heat flux methods were performed with a suite of physical and biogeochemical sensors in both the air and water [*Zemmelink et al.*, 2004; *Schimpf et al.*, 2004; *Garbe et al.*, 2004; *Frew et al.*, 2004]. This region is the largest oceanic source of CO_2, with an annual CO_2 flux of 0.5–1 billion tons of carbon [*Takahashi et al.*, 1993] and shows large interannual variability caused by the ENSO cycle [*Feely et al.*, 1999, 2002, 2004]. The area also experiences lower wind speeds relative to most other ocean regions. Since this area exhibits unique conditions and is of such importance to the global carbon cycle, it is important for the direct determination of fluxes, gas transfer velocities and environmental forcing parameters. This in turn can lead to improved regional parameterizations of gas transfer [*Hare et al.*, 2004]. In this paper, the results of this ambitious and successful study are described.

2. Study Site

[7] GasEx-2001 took place on the NOAA ship *Ronald H. Brown* (*Brown*) in the South Equatorial Current (SEC) in the eastern equatorial Pacific (125°–132°W, 2°–3°S) with the cruise track shown in Figure 1. Extensive pCO_2 measurements had been made in the region on ship surveys and during iron fertilization studies [*Coale et al.*, 1996; *Feely et al.*, 2002]. The area has the highest ΔpCO_2 levels of any open ocean region, with average ΔpCO_2 of 80–150 μatm. High ΔpCO_2 values are persistent, except during the most extreme ENSO conditions. The region has large-scale homogeneity over 100-km sections, particularly in the zonal direction such that the prevailing trade winds cross a large region of similar pCO_2 values.

[8] Similar to GasEx-1998 [*Wanninkhof and McGillis*, 1999; *Hood et al.*, 2001; *McGillis et al.*, 2001a, 2001b; *Feely et al.*, 2002; *Zhang et al.*, 2001], the GasEx-2001 scientific objectives included the measurement of biogeochemical processes in the water column along with ocean and atmospheric physical processes (see accompanying papers in this volume). However, GasEx-2001 environmental conditions were very different. GasEx-1998 occurred in a strong atmospheric CO_2 sink region with prevailing intermediate to high winds. GasEx-2001 occurred in a strong atmospheric CO_2 source region with persistent lower winds and strong surface currents [*Johnson et al.*, 2004]. With lower winds and large heat fluxes, significant diurnal temperature variations typically occur at the ocean surface and have a significant effect on the gas fluxes.

[9] The *Brown* followed an array of drifting platforms, from YD 45–60 in the equatorial Pacific starting at 125°W, 3°S and ending at 132°W, 2.5°S, covering a distance of 715 km. Two butterfly pattern surveys were conducted during the course of the experiment on YD 45 and YD 52 (Figure 1). These butterfly surveys were used to map the broader oceanographic hydrography and pCO_2 conditions. The periodic ship departures from the drifter track correspond to ship waste release so that the study site was not contaminated.

3. Platforms

[10] Extensive use of autonomous sensors on surface platforms investigated near-surface processes to avoid the surface perturbations caused by the large ship (Figure 2). The surface platforms were also used to determine horizon-

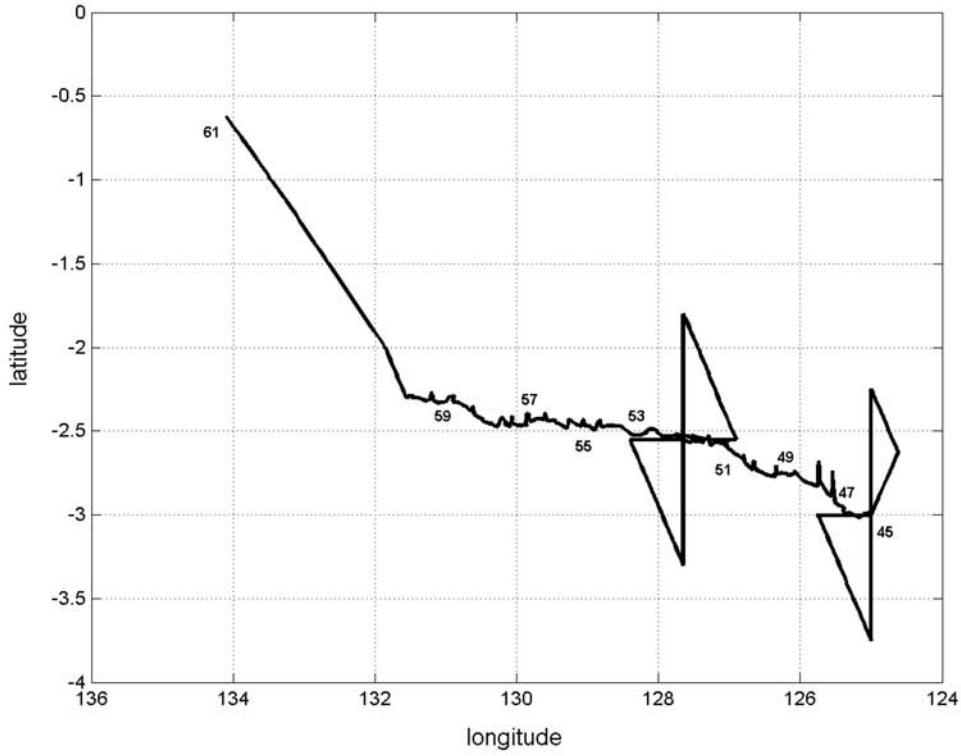

Figure 1. The cruise track of the NOAA ship *Ronald H. Brown* during GasEx-2001. The track line is labeled with YD positions. The process study started on YD 45 at 125°W, 3°S and ended on YD 60 at 132°W, 2.5°S. On YD 45 and YD 52, two butterfly pattern surveys were conducted during the course of the Lagrangian experiment. The surveys were conducted to obtain an understanding of the broader hydrography and pCO_2 climatology and variability thereof.

tal variability by comparison to ship-based measurements and served as water mass markers to facilitate a Lagrangian study. The drifting surface platforms responded to both the near-surface currents and the wind field. The process study was thus conducted in a moving Lagrangian frame with coincident measurements from all platforms.

[11] The surface processes instrument platform (SPIP) is a 15-foot, remotely operated Hobie Wave catamaran used to measure the atmospheric profiles of CO_2, temperature, water vapor, and momentum very close to the air-water interface (Figure 2). SPIP has the advantage of measuring the atmospheric boundary layer near the surface with less flow distortion than the *Brown*. SPIP has fixed atmospheric sensors at the top of its mast while a second set of identical sensors are mounted to a motorized traveler that covers 30 cm to 3 m above the water surface. The measured profiles are used to calculate the CO_2, latent, sensible, and momentum fluxes as well as the appropriate transfer coefficients for comparison to the direct covariance measurements and bulk formulae. During the experiment, the *Brown* followed the drifter array consisting of the air-sea interaction spar (ASIS) buoy (Figure 2), the CARIOCA pCO_2 buoy [*Merlivat and Brault*, 1995], and a SAMI-CO_2/YSI chain [*DeGrandpre et al.*, 2004]. The YSI sensors measured oxygen, temperature, and conductivity. The drifter array was connected to a subsurface drogue. The CARIOCA was coupled with a single SAMI and a YSI sensor at about 1.5 m. The YSI O_2 sensors failed, and other O_2 sensors had significant but recoverable drift. These buoy-mounted spectrophotometric CO_2 sensors did not perform well during the study because of ambient light interference and biofouling in the water. The ASIS buoy had two SAMI instruments and one YSI sensor at 1.5-m depth, and a SAMI at 5-m depth. The drogue had two SAMI instruments with two YSI sensors at 4 and 30 m and two O_2 sensors at 10 and 15 m. Two GPS/Argos trackers were mounted on CARIOCA, one on ASIS, and one on the GPS buoy on the drogue.

4. Measurement Systems

4.1. Atmospheric Measurements

[12] Meteorological and turbulent flux measurement systems were mounted on the *Brown*, ASIS, and SPIP. Direct covariance flux measurements were performed from the *Brown* and ASIS. Flux profile measurements were performed from the *Brown* and SPIP. Direct covariance flux systems are capable of correcting for the velocity of platform motion [*Edson et al.*, 1998; *Drennan et al.*, 1999] but measurement of the true vertical wind velocity is needed to compute the covariance fluxes. On the *Brown*, a Solent three-axis ultrasonic anemometer-thermometer and a Systron-Donner MotionPak system of three orthogonal angular rate sensors and accelerometers were used. The MotionPak was mounted directly beneath the sonic anemometer, allowing for accurate alignment with the sonic axes in addition to ensuring that the wind and motion measurements were collocated. Long- and short-wave radiation and barometric pressure were supplied by the IMET system onboard the *Brown*. During GasEx-

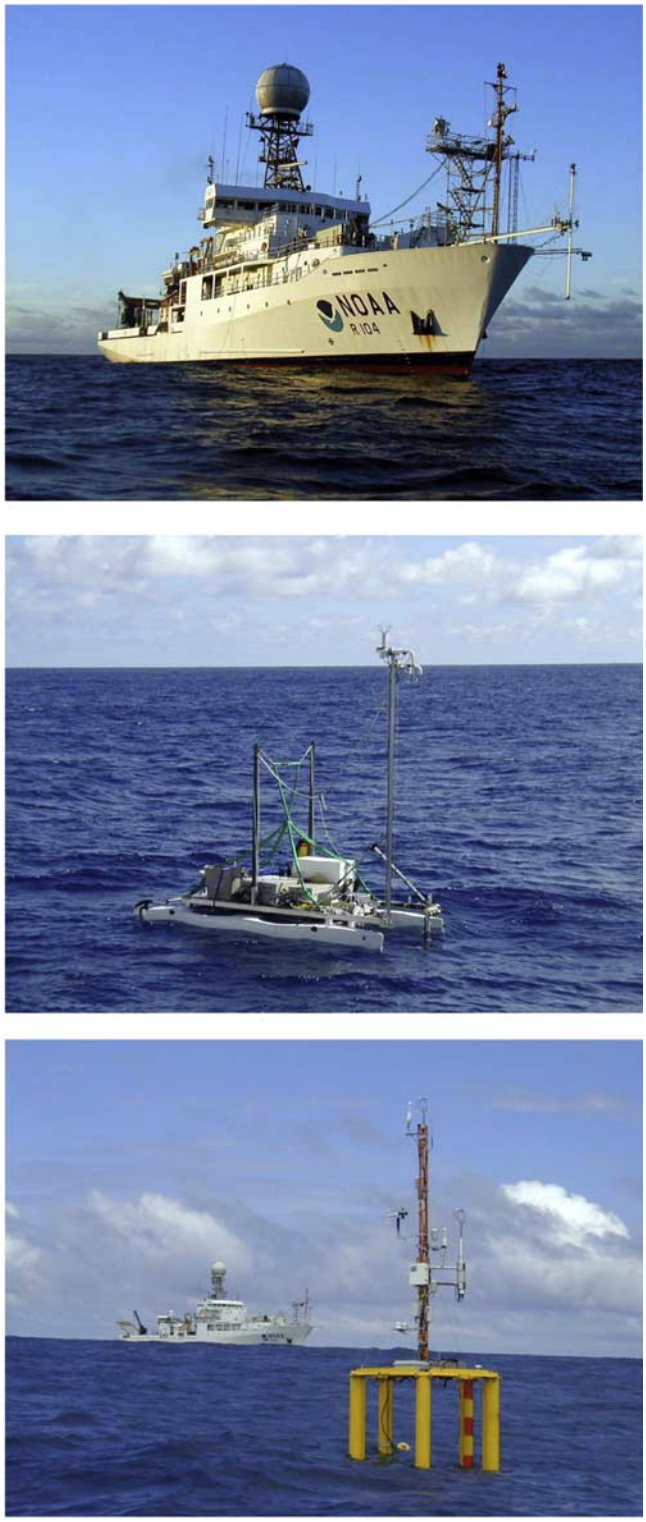

Figure 2. Floating platforms used to support flux and surface process measurements during GasEx-2001: (top) *Brown*, (middle) SPIP, and (bottom) ASIS.

2001, the shipboard micrometeorological system was deployed at the end of a 10-m bow boom (Figure 2). This placed the anemometer 9 m above the mean sea surface. The boom system was similar to that mounted on the R/V Franklin [*Bradley et al.*, 1991].

[13] Both fixed and profiling sensor packages were deployed at the end of the *Brown* bow boom for mean meteorological measurements. Each package was aspirated and included a combined thermocouple, RH-temperature, and CO_2/H_2O measurement. The thermocouple was a Campbell Scientific Model ASPTC. The RH-temperature sensor was a small Vaisala model HMP233. The profiling system included an aspirated relative humidity-temperature sensor and an aspirated thermocouple. Closed path NDIR sensors were also part of the shipboard meteorological system. The precision of the NDIR sensors are a function of detector temperature fluctuations and therefore the closed path NDIR systems were mounted within a temperature-controlled, stainless steel, environmental chamber located in a shrouded housing. A 5000 BTU air conditioner removed heat to the outside. Tube lengths from the end of the boom to the detectors were 15 m. A LI7000 sensor sampled air through a tube attached to the fixed sensor package. A LI6262 sampled air from the profiling aspirator on the mast.

[14] Profiles of temperature, water vapor, and CO_2 were obtained using the suite of sensors and intake tubes moving up and down an 8-m mast at the end of the bow boom. The top and bottom of the mast were located nominally 12 and 4 m above the mean sea surface, respectively. The profile measurements were referenced against a fixed suite of sensors located at 9 m. These sensors were used to remove naturally occurring variability during the profiling periods as described below. Each profile took 1 hour to complete. Naturally occurring horizontal variability over this sampling period generated differences that were often larger than the differences over the vertical profiles [*McGillis et al.*, 2001b].

4.2. CO_2 Measurements

[15] The main underway pCO_2 system used the equilibrator NDIR method [*Weiss*, 1974; *Wanninkhof and Thoning*, 1993]. The large showerhead equilibrator contained about 8 L of water and 16 L of headspace. The water was pumped to the equilibrator at a rate of 40 L min^{-1} from nominally 5-m depth from the bow and was transferred through 100 m of Teflon lined tubing to the laboratory housing the system. About 10 L min^{-1} was diverted to the showerhead of the equilibrator. The system ran on an hourly cycle during which three reference gases were analyzed that spanned the observed water fCO_2 range followed by analysis of equilibrator headspace samples at 3.5-min intervals. Three ambient air samples were obtained at similar intervals and the hourly cycle was completed with more water fCO_2 samples. All the analyses were referenced to standards directly traceable to the WMO scale and provided by NOAA's Climate Monitoring and Diagnostic Laboratory [*Conway et al.*, 1994].

4.3. Surface and Subsurface Instrumentation

[16] In addition to underway pCO_2 and ocean bulk temperature, subsurface measurements on the *Brown* included a 150-kHz acoustic Doppler current profiler (ADCP). A laser altimeter and a microwave wave height sensor were deployed off the *Brown* bow boom. The drogue drifter chain, ASIS, and SPIP included additional surface and subsurface instrumentation. A downward looking 1200-kHz ADCP, two 10-MHz acoustic Doppler current velocimeters (ADVs), and a YSI sensor were deployed on SPIP at 0.5-m depths. ASIS was equipped

with arrays of capacitance wave wires, thermistors, and ADVs, along with a downward looking 600-kHz ADCP.

5. Results and Discussion

5.1. Environmental Conditions

[17] A summary of the environmental conditions observed during the 15-day process study is shown in Figures 3 and 4. Wind speed was low and relatively constant at 6.1 ± 1.3 m s^{-1}. Other atmospheric and oceanic properties were relatively steady. The ΔpCO_2, solar incidence, barometric pressure, and bulk temperature show obvious diurnal cycles. The wind speed (Figure 3) and wave field (Figure 4) do not show substantial diurnal variations. The wave field was dominated by swell waves propagating from the north to northeast at roughly 45°–90° from the wind.

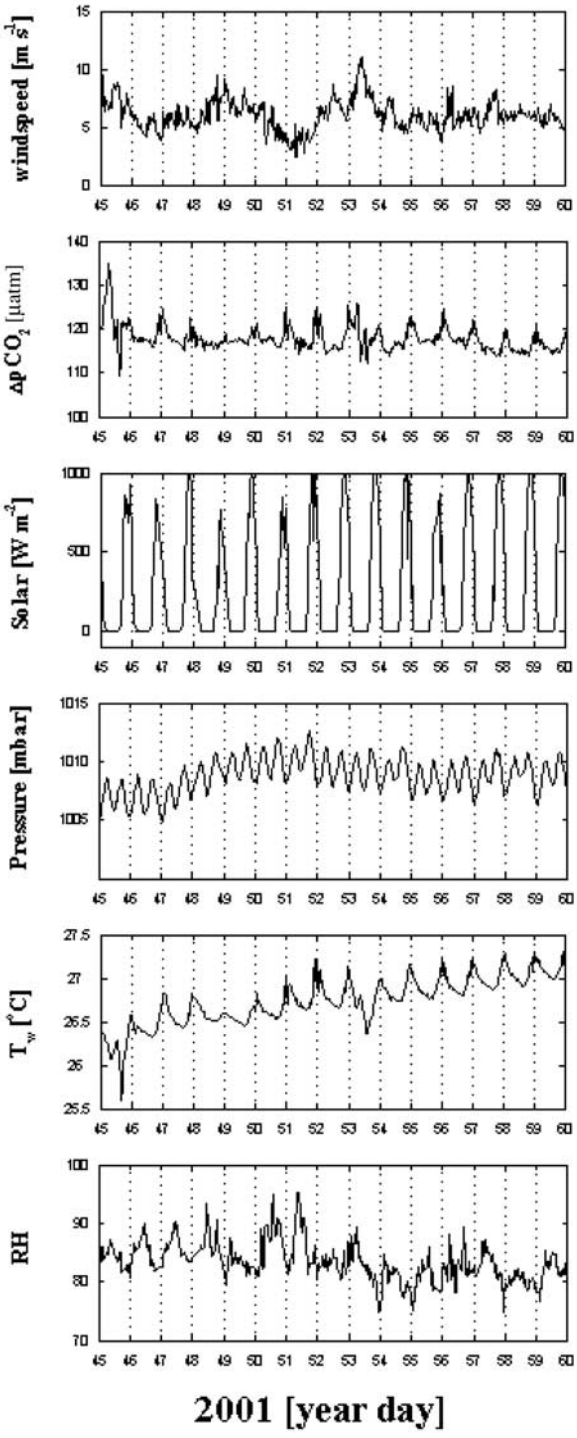

Figure 3. Process study time series of wind speed, ΔpCO_2, solar incident radiation, barometric pressure, bulk water temperature, and atmospheric relative humidity.

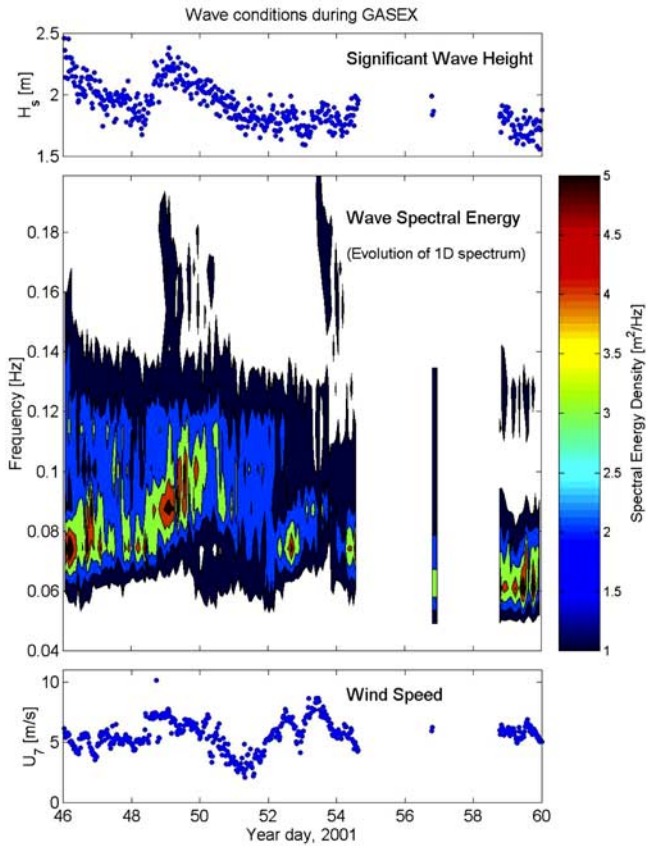

Figure 4. Time series of surface wave measurements from ASIS. The significant wave height is calculated from the spectral energy of the wave field. The wind speed is measured from the ASIS buoy.

[18] Near-surface thermal and density gradients have been extensively studied in the equatorial Pacific because of the region's considerable influence on heat and fresh water fluxes, for instance in the TOGA/COARE experiment [*Fairall et al.*, 1996b]. The sea surface temperature variations during GasEx-2001 were established over periods of hours because of the large heat fluxes and low winds. Two counteracting thermal processes occurred under these conditions: (1) since radiation is absorbed over the top several meters of the water column but released right at the surface, a heat balance requires the very surface to cool [*Fairall et al.*, 1996a; *Schlüssel et al.*, 1990; *Soloviev and Schlüssel*, 1994]; (2) the upper ocean also heated during the daytime causing a diurnal mixed layer. Both effects influence the ΔpCO_2 and the diurnal gas fluxes [*McNeil and Merlivat*, 1996; *Robertson and Watson*, 1992; *Van Scoy et al.*, 1995; *Ward et al.*, 2004].

5.2. Surface Fluxes

5.2.1. Direct Covariance Flux Method

[19] The flux determined by the micrometeorological methods assumes stationary conditions over the measurement period and knowledge of the atmospheric boundary layer stability. The inferred fluxes are critically dependent on these assumptions. The stationarity criteria for micrometeorological fluxes will be violated if there are horizontal gradients in the air over the area of measurements [*Businger and Delaney*, 1990]. This requires the signal averaging duration to correspond to as much as 50 km. Over the open ocean, variability in the air CO_2 concentration will be a function of the variability in pCO_2 in the surface water and the effect from remote land sources, although the influence of the latter will result in more gradual and likely insignificant changes.

[20] The corrected velocity components are used to compute the covariance fluxes of momentum, gas, sensible heat, and water vapor. The momentum flux is described by

$$\tau = -\rho\overline{u'w'}, \tag{1}$$

where the overbar represents a time average quantity, ρ is the density of moist air, and u and w are the horizontal and vertical wind velocity components, respectively. In this expression, u' and w' represent the turbulent fluctuations. The surface friction velocity can be directly derived from the direct covariance by

$$u* = \left(-\overline{u'w'}\right)^{1/2}. \tag{2}$$

The turbulent air-sea fluxes for sensible, H_s, and latent, H_l, heat can also be measured using w' with fluctuating temperature and water vapor concentrations, giving

$$H_s = \rho c_p \overline{w'T'}, \tag{3}$$

$$H_l = \rho L_E \overline{w'q'}, \tag{4}$$

where c_p is the specific heat for moist air, L_E is the water latent heat of vaporization, T is the air temperature, and q is the specific humidity.

[21] The direct covariance measurement technique is a standard for surface layer gas flux measurements as it is a direct computation of the covariance of the gas concentration with the air vertical velocity at the height of measurement. With an accurate estimate of the vertical velocity signal, the gas flux is computed by correlating the true vertical wind velocity with atmospheric CO_2 concentrations. The accuracy of this flux is therefore dependent on the sensitivity of the gas analyzer to high-frequency fluctuations. Fast response measurements of CO_2 are used to directly estimate the CO_2 flux,

$$F_{CO2} = \overline{w'c'}, \tag{5}$$

where c' is the fluctuating atmospheric mixing ratio of CO_2 in dry air. The shipboard flux system deployed in GasEx-2001 was a modification of the direct covariance flux system used to measure CO_2 fluxes during GasEx-1998 [*McGillis et al.*, 2001a]. With regard to implementing the direct covariance method for CO_2, the greatest challenges centered around: (1) the presence of adequate fluctuation levels in w and c to compute the gas flux using currently available sensors, and (2) the ability to adequately remove the motion contamination and minimize the effect of flow distortion around an oceangoing vessel. The momentum flux is very sensitive to motion contamination because it requires corrections to both the vertical and horizontal velocities as opposed to the scalar, including gas, fluxes that are mainly influenced by uncertainties in the vertical velocity. Detection of CO_2 concentrations using NDIR analyzers is also susceptible to errors due to water vapor absorption [*Webb et al.*, 1980; *Fairall et al.*, 2000; *McGillis et al.*, 2001a]. All direct covariance measurements thus require null tests to assess the effect of motion and water vapor concentrations on fluxes. The null test to quantify motion errors was performed by supplying constant CO_2 to the detectors and quantifying the artifact fluctuations. The null test to quantify water vapor errors was performed by supplying constant CO_2 to the detectors with varying water vapor content. In both null tests, corrections are determined to account for motion and water vapor artifacts.

[22] Time series of momentum, heat, and CO_2 direct covariance fluxes are shown in Figure 5. The flux variability was caused by environmental forcing and measurement uncertainty. Because wind speed variability was small, diurnal processes were the origin of most of the variability in the atmospheric and oceanic forcing. The most significant diurnal process is the heating and cooling of the ocean surface. The surface ocean is heated during the day by incident solar radiation. At night, when solar radiation is nonexistent, infrared radiation, evaporation, and sensible heat fluxes cool the ocean surface. These processes vary through the diurnal cycle and cause subsequent processes that change the transport of heat, mass, and momentum across the air-sea interface. The diurnal barometric pressure changes are small. Thus the time series of direct covariance measurements are close to a uniform daily mean and banded around variability caused by noise and diurnal forcing. The mean and standard deviation of momentum, latent, sensible, and CO_2 direct covariance fluxes were -0.058 ± 0.036 N m^{-2}, 83.2 ± 51.3 W m^{-2}, 4.4 ± 7.1 W m^{-2}, and 3.9 ± 3.1 mol m^{-2} yr^{-1}. Note that the standard deviations of the measured half-hour direct covariance fluxes are often as large as the mean fluxes.

5.2.2. CO_2 Flux Profile Method

[23] Since the flux profile technique relies on the mean gradients in the atmospheric boundary layer, it offers several advantages in determining air-water fluxes. The flux profile technique averages over small spatial and temporal scales (m^2 and min, respectively), which are necessary because winds, tides, surfactants, and diurnal processes may change on small scales. With the proposed ancillary information from the direct covariance method, the Monin-Obukhov length can be determined. This decreases the uncertainty in calculating the gas transfer velocity, k, using the flux profile technique through a better characterization of the atmospheric surface layer (ASL).

[24] The flux profile method relies on measuring vertical gradients of CO_2 in the ASL. Monin-Obukhov (M-O) similarity theory can be used to describe turbulent properties in the surface layer [*Panofsky and Dutton*, 1984]. In a

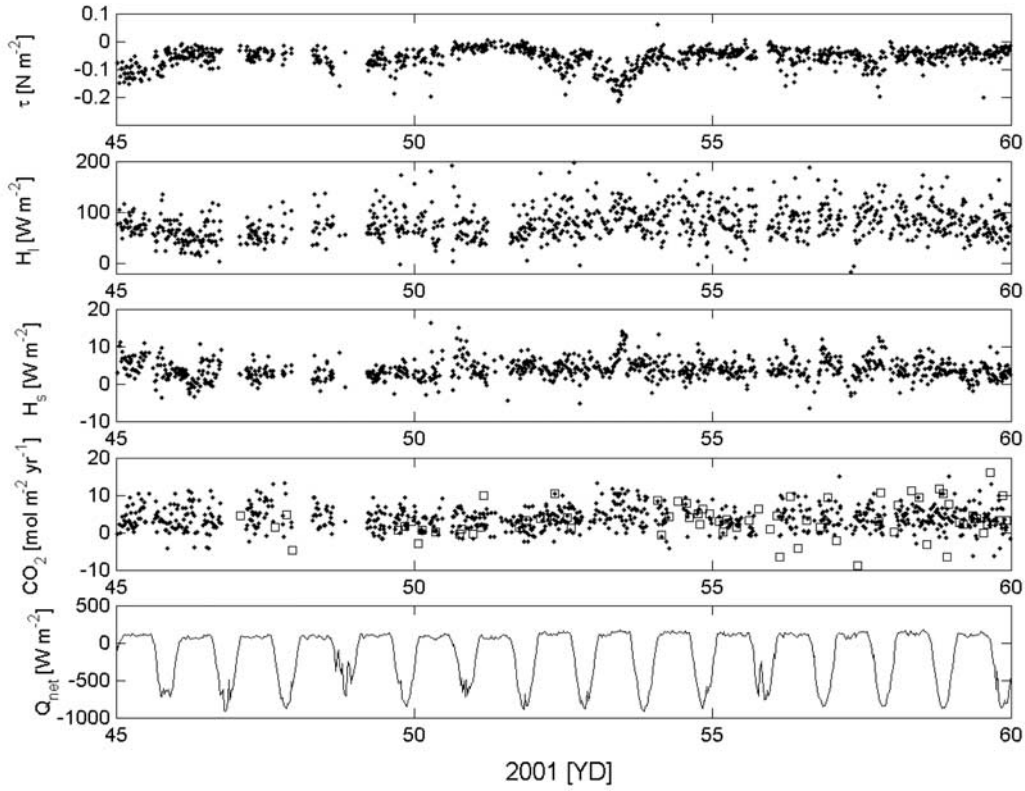

Figure 5. Process study time series of measured air-sea fluxes. Direct covariance fluxes (solid circles) of momentum (τ), latent heat (H_l), sensible heat (H_s), and CO_2 (F_c) are shown. CO_2 profile fluxes are also shown for comparison (open squares). The net air-sea heat flux (Q_{net}) indicates the strong diurnal forcing.

surface layer where the flow is driven by mechanical (shear) and thermal (buoyancy) forcing, M-O similarity shows that various turbulence statistics, when normalized by an appropriate scaling parameter, are universal functions of z/L, where z is the height above the water surface and L is the M-O scaling length. The M-O length is defined by

$$L = -\frac{\overline{T_v}}{\kappa g}\frac{u_*^3}{F_{T_v}}, \tag{6}$$

where g is the acceleration of gravity, T_v is the virtual temperature, F_{T_v} is the buoyancy flux, u_* is the friction velocity, and κ is the von Kármán constant, assumed to equal 0.4. The M-O length represents the ratio of mechanical to thermal forcing, and the height where $z = L$ represents the height at which these two forcing mechanisms are equal.

[25] The flux profile method is related to the direct covariance flux by

$$\overline{w'c'} = -K_c\frac{dc}{dz}, \tag{7}$$

where K_c is the atmospheric diffusivity for CO_2 defined as

$$K_c = \frac{u_*\kappa z}{\phi_c(\xi)}, \tag{8}$$

where ϕ_c is an empirically determined dimensionless gradient function for c [e.g., *Paulson*, 1970] and the stability parameter is $\xi = z/L$. Averaged atmospheric profiles of dry mole fraction of CO_2 (xCO_2) are shown in Figure 6 for the *Brown* and SPIP. Measurements from the *Brown* mast were taken from 4 to 12 m above the sea surface. SPIP measurements could be made from the water surface at 0.5 and 3 m.

[26] *Edson et al.* [2004] tested the flux profile relationships for water vapor and temperature during GasEx-2001. An expression for ϕ_c based on water vapor and temperature profiles during GasEx-2001 is given by Edson et al.:

$$\phi_c\left(\frac{z}{L}\right) = \left(1 - 13.4\frac{z}{L}\right)^{-1/2}. \tag{9}$$

Figure 7 shows the scalar flux profile relationship, equation (9), and data from GasEx-2001. Edson et al. provide a first test of overland models [*Dyer*, 1974] applied to open ocean conditions and allow for the implementation of M-O and flux profile methods to CO_2 fluxes.

[27] Integrating the flux equation, a semilogarithmic profile is obtained

$$\overline{c}(z) - \overline{c}(z_{oc}) = \frac{c_*}{\kappa}[\ln(z/z_{oc}) - \psi_c(\xi)], \tag{10}$$

where ψ_c is the integral form of ϕ_c, $\overline{c}(z_{oc})$ represents the surface value of c, and z_{oc} is the surface roughness length for c. The integral form is given as

$$\psi_c(\xi) = \int [1 - \phi_c(\xi)]\frac{d\xi}{\xi}. \tag{11}$$

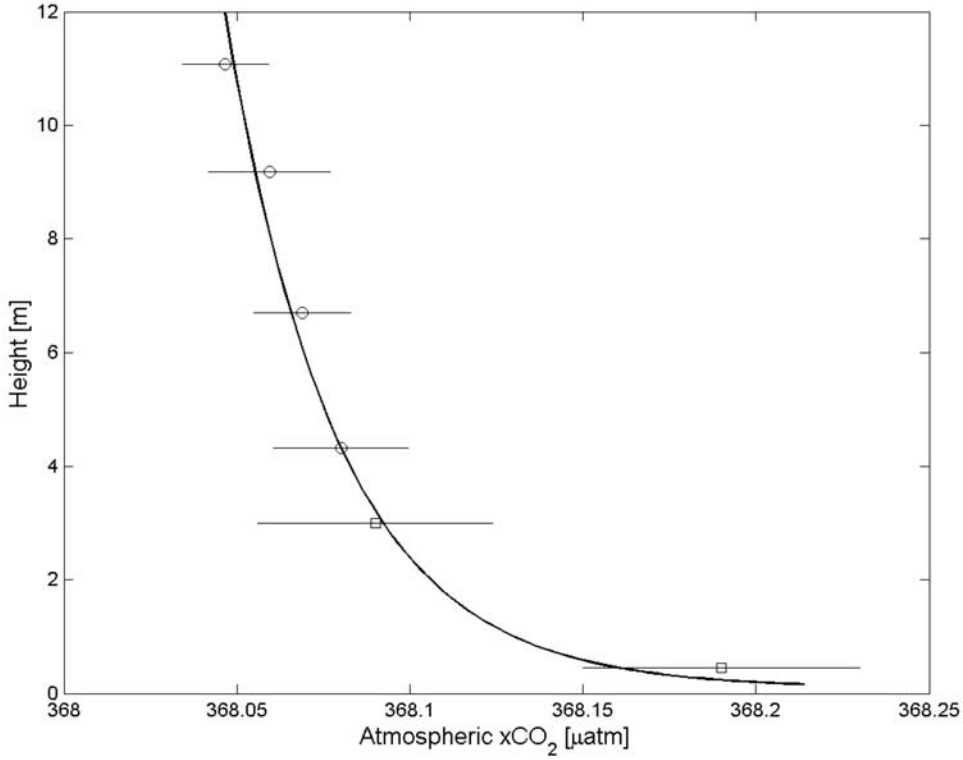

Figure 6. Ensemble atmospheric xCO_2 profile collected during the cruise from masts on the ship (open circles) and SPIP (open squares). The semilogarithmic fit (solid line) is used to calculate air-sea exchange using the flux profile relationships. Horizontal bars indicate standard deviation error bars.

[28] The M-O length is measured using the direct covariance fluxes during GasEx-2001, and the scaling parameter ($c_* = F/u_*$) and roughness length (z_{oc}) can be determined as the slope and intercept of equation (10). Note that the stability parameter can also be determined in an iterative fashion by the profile method alone if the gradients of velocity, temperature, and water vapor are also measured. The flux is then calculated by combining this scaling parameter with the friction velocity. Using equation (1), this flux estimate is used, along with measurements of the air-water concentration gradient, to calculate k [*McGillis et al.*, 2001b].

[29] Equations (10) and (11) were used to construct a time series of atmospheric xCO_2 profiles for GasEx-2001 (Figure 8). Variability in the atmospheric xCO_2 structure is a result of air-sea CO_2 flux variability as well as atmospheric stability. Because of this, the atmospheric xCO_2 gradient increases with an increase in CO_2 flux and a decrease in momentum flux. The atmospheric xCO_2 gradient also increases when the atmospheric stability increases.

5.2.3. CO_2 Bulk Transfer Method

[30] The bulk transfer method provides an estimate of fluxes between the ocean and atmosphere using mean, or bulk, exchange quantities and parameterized exchange rates. In the common bulk form, the CO_2 flux F_{CO_2} is expressed as

$$F_{CO_2} = k_{660}\ \Delta CO_{2aq} (Sc_{CO_2}/660)^{-n}, \qquad (12)$$

where k_{660} represents the gas transfer velocity referenced to Sc = 660, ΔCO_{2aq} is the difference between the concentration of aqueous dissolved CO_2 in the bulk seawater and at the ocean surface, Sc_{CO_2} is the CO_2 Schmidt number, and n is a hydrodynamic variable adjusted for flow condition. For the GasEx-2001 data analysis, the value of $n = 0.5$ was used. This was a reasonable approximation due to the small amount of surface films in this region. CO_2 is a waterside controlled gas [*Liss and Slater*, 1974; *Businger*, 1997;

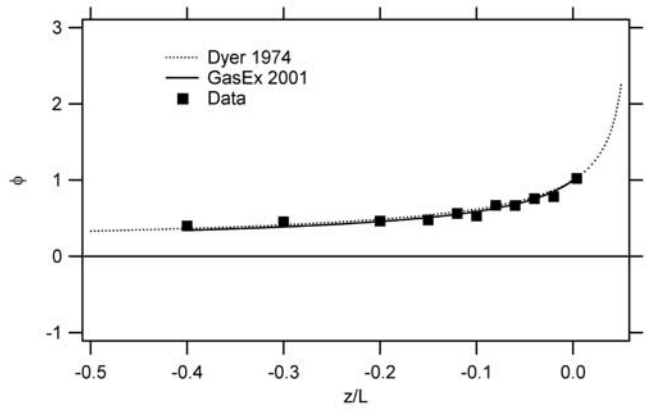

Figure 7. Water vapor flux profile relationship for GasEx-2001 [*Edson et al.*, 2004]. The flux profile relationship is calculated from coaligned direct covariance water vapor fluxes and atmospheric water vapor profiles measured from the shipboard mast system. The GasEx-2001 data (solid squares) are compared to the model of *Dyer* [1974] (dotted line). A fit to the measured data is also shown for comparison (solid line).

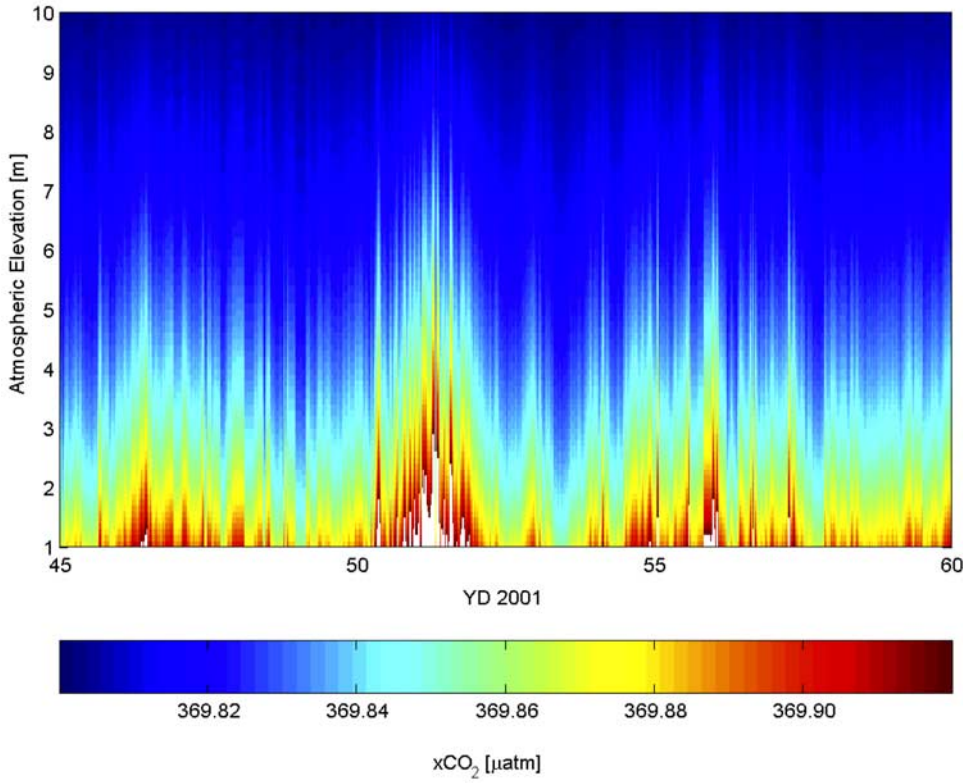

Figure 8. Calculated time series of atmospheric xCO_2 profiles.

McGillis et al., 2000]; therefore the surface concentration $CO_{2aq,s}$ can be closely approximated by the measured airside partial pressure of CO_2, pCO_{2a}, defined as $pCO_{2a} = xCO_{2a}$ (P-p_{H2O}) where P is the ambient pressure and p_{H2O} is the water vapor pressure. Thus

$$\Delta C_{CO_2} = CO_{2aq,w} - spCO_{2a}, \tag{13}$$

where s is the solubility, which depends on surface temperature and salinity at the surface. $CO_{2aq,w}$ is the bulk water aqueous CO_2 determined from TCO_2 and pCO_{2w} [*Peng et al.*, 1987]. pCO_{2w} and pCO_{2a} are the partial pressures of CO_2 in the ocean and atmosphere, respectively. The concentration difference across the aqueous boundary layer is used rather than the more commonly used expression of partial pressure gradient because the pCO_{2w} at the surface is not well quantified in an environment with strong vertical temperature gradients [*Ward et al.*, 2004]. Figure 9 shows the time series for $CO_{2aq,s}$, $CO_{2aq,w}$, and ΔCO_{2aq} during GasEx-2001. The concentration difference driving exchange, $\Delta CO_{2aq} = CO_{2aq,w} - CO_{2aq,s}$, shows small diurnal variability in the mean. Diurnal increases in ΔCO_{2aq} are predominantly caused by decreases in the daytime $CO_{2aq,s}$ as a result of decreased solubility.

[31] Figure 10 shows the CO_2 flux results from GasEx-2001. Bin-averaged and raw direct covariance, flux profile, and gas exchange wind speed models of CO_2 flux are plotted versus wind speed. Model fluxes use a mean ΔCO_{2aq} value of 3.2 µmol L^{-1} in equation (12). This is a good approximation since the standard deviation of ΔCO_{2aq} is only 0.05 µmol L^{-1}. Data is plotted in comparison to other wind speed relationships [*Liss and Merlivat*, 1986; *Wanninkhof*, 1992; *McGillis et al.*, 2001a, 2001b].

[32] Transfer coefficients, or the Dalton number, are used to compare the aerodynamic form of CO_2 with H_2O. These bulk transfer coefficients for water vapor, C_E, and a slightly soluble gas, C_G, are expressed as

$$C_E = \frac{H_l}{\rho_a L_E \left[Q_{z_{oq}} - Q_{10}\right] U_{10}} \tag{14}$$

$$C_G = \frac{F_G}{\left[C_{aq,w} - C_{aq,s}\right] U_{10}} \cdot \left[\frac{Sc_G}{660}\right]^{1/2}, \tag{15}$$

where H_l and F_G are the latent heat (Wm^{-2}) and surface gas flux (mol m^{-2} yr^{-1}), respectively. The subscript 10 is the reference 10-m atmospheric quantity and the subscript s refers to the surface, or interfacial, quantity. The gas transfer coefficient is given as a referenced Schmidt number = 660.

[33] Figure 11 shows C_E and C_G for GasEx-2001. Air-sea temperature differences were typically less than 1°C and the values for C_E ranged from $0.8-3 \times 10^{-3}$, consistent with values previously reported [*Kondo*, 1975; *Bradley et al.*, 1991; *Fairall et al.*, 1996a, 1996b]. The scatter in measurements is typical of direct covariance observations. However, binned data of C_E show this technique provides a good agreement with the parameterizations of the TOGA/COARE model. The CO_2 exchange coefficients are also shown in Figure 11. Cubic and quadratic parameterizations

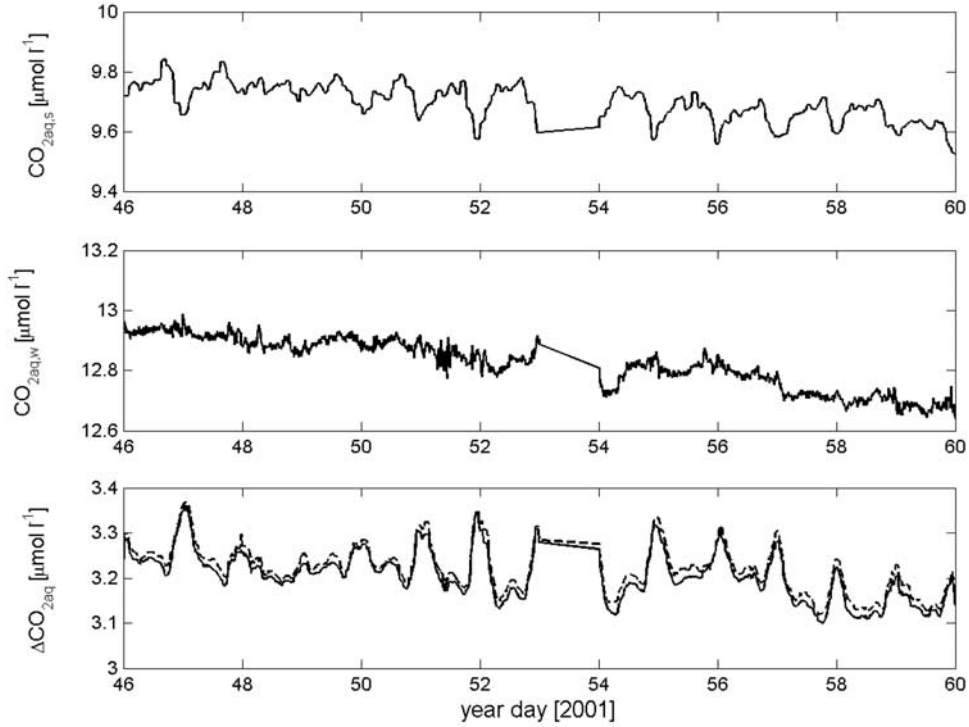

Figure 9. Time series of CO_2 concentrations driving air-sea CO_2 exchange. $CO_{2aq,w}$ is the aqueous CO_2 concentration in the bulk water. $CO_{2aq,s}$ is the CO_2 concentration on the ocean surface. The concentration difference driving exchange, $\Delta CO_{2aq} = CO_{2aq,w} - CO_{2aq,s}$, shows small variability in the mean. The diurnal increases in $\Delta CO_{2aq,w}$ are predominantly caused by decreases in the daytime $CO_{2aq,s}$. The ΔCO_{2aq} using surface temperature (dashed line) is shown for comparison.

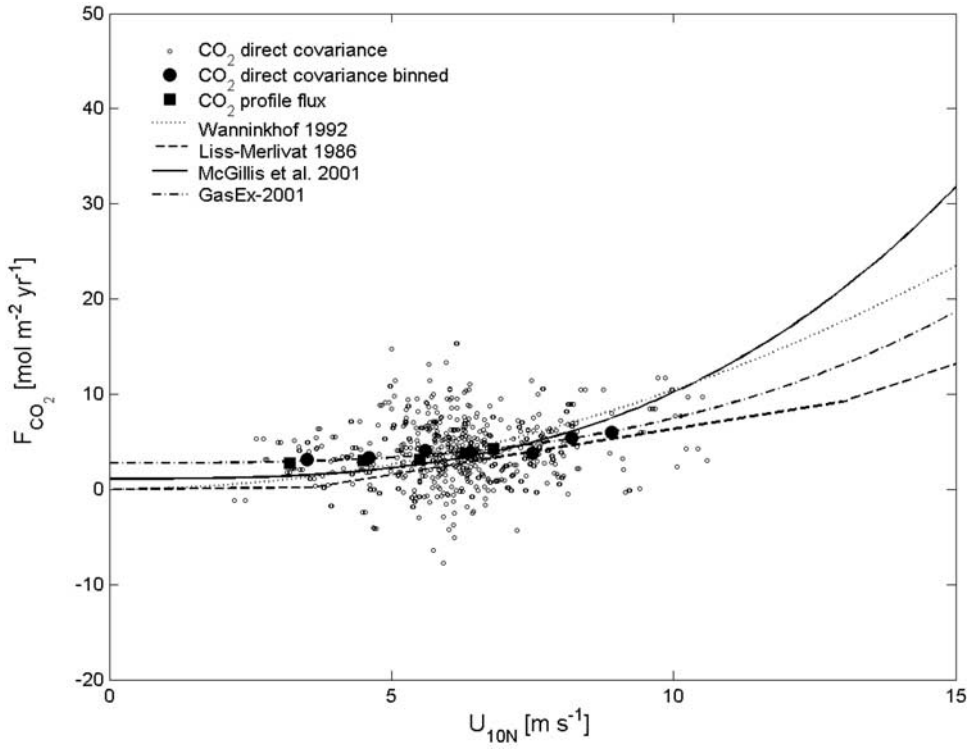

Figure 10. GasEx-2001 micrometeorological CO_2 fluxes. The half-hour direct covariance (DC) fluxes are compared to the ensemble-averaged DC fluxes (solid circles). The flux profile CO_2 fluxes are shown for comparison (solid squares). Wind speed-dependent gas exchange models are used with a mean CO_2 difference of 3.20 µmol^{-1}.

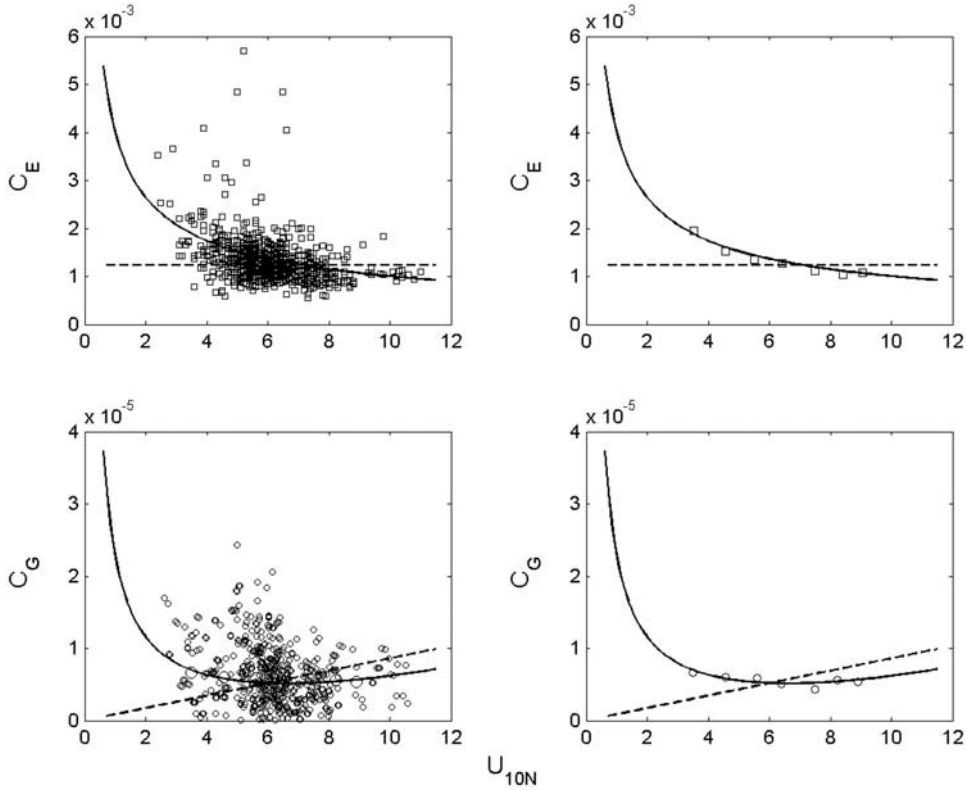

Figure 11. Surface exchange coefficients for H_2O (C_E) and CO_2 (C_G). (left) Raw values and (right) bin-averaged values are shown for both H_2O and CO_2. For H_2O comparisons, *Kondo* [1975] (dashed line) and TOGA/COARE (solid line) lines are given. For CO_2 comparisons, *Wanninkhof* [1992] (dashed line) and a cubic fit (solid line) are shown.

are shown for comparison. The expression for the quadratic parameterization [*Wanninkhof*, 1992] is given as

$$C_{G,W-92} = 0.31 U_{10} (Sc/660)^{1/2}. \quad (16)$$

As shown in Figure 11, this expression is linear for wind speed.

[34] Bin-averaged gas transfer velocities are plotted in Figure 12. The *Liss and Merlivat* [1986], *Wanninkhof* [1992], *McGillis et al.* [2001a, 2001b], and a GasEx-2001 fit are plotted for comparison. Also plotted for comparison are recent equatorial Pacific deliberate tracer results [*Nightingale et al.*, 2000]. A regression for the gas transfer data with wind speed gives $k_{660} = 8.2 + 0.014\ U_{10N}^3$. The greatest convergence of data and models exists near a 6 m s^{-1} wind speed. Data suggest an elevated gas transfer velocity at wind speeds less than 6 m s^{-1} and a very weak dependence on wind speed (Figure 10). Chemical enhancement may play a role in increasing measured gas transfer velocities in the equatorial Pacific. The canonical values suggest smaller enhancement than observed. The enhancement under the conditions present in GasEx-2001 is calculated to be less than 5% [*Wanninkhof and Knox*, 1996]. Other environmental factors unique to the equatorial Pacific may also modulate low-wind gas exchange. These may include surfactant characteristics, consistent currents, and diurnal forcing, as discussed below.

[35] At low winds, surfactants are known to modulate gas exchange because of dampening of waves and turbulence [*Jähne et al.*, 1987; *Frew*, 1997; *Bock et al.*, 1999; *McKenna and McGillis*, 2004]. The GasEx-2001 study site was very remote with no direct anthropogenic influence nor significant biological activity, two main surfactant sources. This results in a region with low CDOM levels [*Siegel et al.*, 2002] and indiscernible background surface films. Thus surfactant dampening of waves and turbulence was unlikely to have occurred during GasEx-2001. As a result of the lack of surface films in this study region, higher values of k at a given wind speed may be expected. An approximate increase greater than a factor of 2 would be expected over most areas of the ocean that experience discernible amounts of surface films [*Frew*, 1997; *Bock et al.*, 1999]. However, the lack of surfactants cannot explain the very weak dependence on wind speed and additional explanations must be sought.

5.3. Diurnal Processes

[36] The physical and biogeochemical climatology in GasEx-2001 was unique because the diurnal cycling was very consistent. GasEx-2001 provided an environment to explore diurnal physical, chemical, and biological processes by analyzing daily averages of the data. Figures 13–16 show the effect of diurnal cycles on the properties controlling CO_2 flux. Average diurnal trends show a small variation in wind speed with a strong cycle in solar incidence giving rise to a diurnal cycle of many processes. The effect of the diurnal cycle on surface ocean heat and momentum fluxes has been previously described [e.g., *Price et al.*, 1986; *Kantha and Clayson*, 1994].

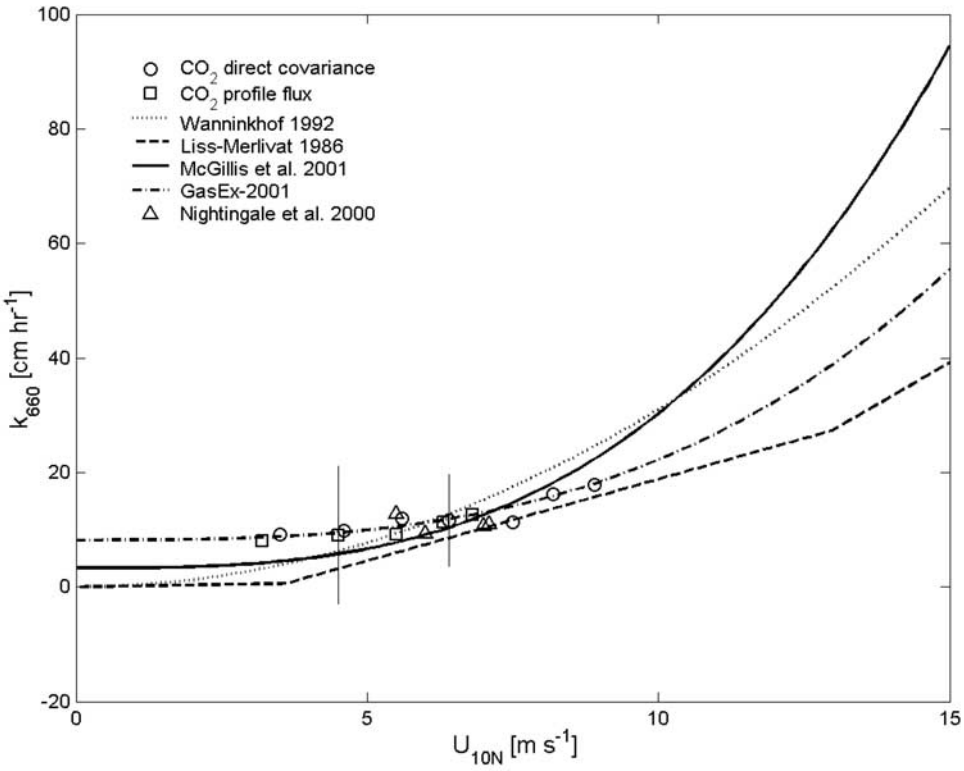

Figure 12. GasEx-2001 k_{660} for CO_2 data from direct covariance (DC) and flux profile (FP) methods. The dashed line corresponds to the bulk method of *Liss and Merlivat* [1986]. The dotted line corresponds to the bulk method of *Wanninkhof* [1992]. The solid line is the bulk method from *McGillis et al.* [2001a, 2001b]. The dash-dotted line is the cubic fit to the GasEx-2001 data. The equatorial Pacific deliberate tracer gas exchange values from *Nightingale et al.* [2000] are shown for comparison. Vertical bars indicate standard deviations.

[37] Figure 13 shows the barometric pressure exhibited during a diurnal variation caused by atmospheric tides. Nighttime cooling resulted in a decrease in both air temperature and ocean temperature. The mean diurnal ocean temperature was greater than the air temperature with a small increase in the difference at night. The relative humidity also increased at night. These coherent diurnal processes result in a nighttime decrease in pCO_2. An examination of the CO_2 driving the flux is also shown in Figure 13, where the bulk $CO_{2aq,w}$ shows indiscernible diurnal variation. However, the surface, or skin, $CO_{2aq,s}$ increases at night predominantly because of an increase in gas solubility as a result of cooler surface water.

[38] The diurnal properties have a clear effect on the air-sea CO_2 flux. The diurnal atmospheric gradient of xCO_2 increases at night (Figure 13) and measurements show a 40% increase in nighttime CO_2 flux (Figure 14). Figure 14 also shows that Sc increases by 3% and ΔCO_2 decreases by 2% at night. Because of nighttime cooling of surface water, $Sc^{-1/2}$ decreases by 0.7%. The nighttime ΔCO_2 decreases by 2.5% from the daytime value. Although the diurnal Sc and ΔCO_2 have an additive effect, the combined contribution to increasing nighttime fluxes is small at −2.7%. However, as shown in Figure 14, the nighttime CO_2 flux, F_{CO2}, increased 40% over daytime values.

[39] Using the measured diurnal CO_2 flux, the gas transfer velocity k_{660} was calculated from equation (12). Because the gas transfer velocity was calculated using the diurnal C_{CO2}, the thermal effects on solubility and diffusivity were taken into account. Therefore the residual increase in the gas transfer velocity was attributed to physical processes. For comparison, the gas transfer velocities calculated using the *Soloviev and Schlüssel* [1994] model are plotted in Figure 14. Nighttime increases were calculated using the model based on surface renewal. Also plotted in Figure 14 is the CO_2 flux computed using the wind speed regression from GasEx-2001. There is a contribution of nighttime increase in CO_2 flux due to the diurnal increase in nighttime U_{10N}. The calculations estimate that a 10% nighttime increase in CO_2 flux is due to wind speed alone.

[40] The unique physical processes controlling surface turbulence during GasEx-2001, and tropical regions in general, are notably the large nighttime buoyancy fluxes and daytime trapping of the surface momentum layer. In the diurnal mixed layer, the water friction velocity u_* and the convective velocity w_* contribute to the exchange of momentum [*Imberger*, 1985]. Here, the convective velocity is defined as $w_* = (Bh)^{1/3}$ where

$$\frac{c_p \rho_o B}{g\alpha} = H_s + H_l + q(D) + q(M) - \frac{2}{h}\int_M^D q(z)dz \qquad (17)$$

and c_p and ρ_o are the specific heat and density of water, B is the surface layer heat flux [*Imberger*, 1985], α is the thermal expansion coefficient, q is the net radiation at the surface D and base of the mixed layer M, and h is the diurnal mixed

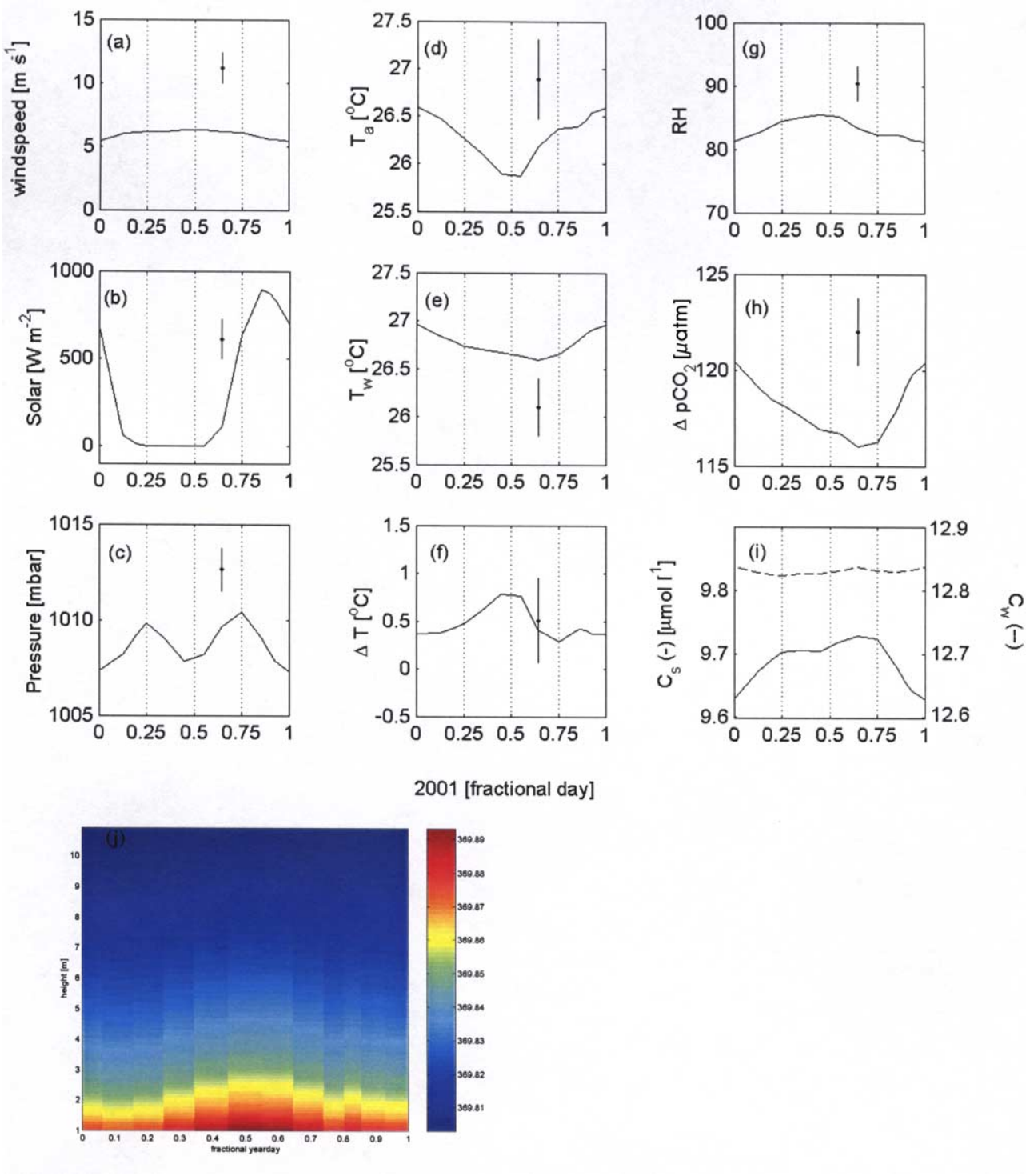

Figure 13. Diurnal variability of (a) wind speed (m s^{-1}), (b) incident solar radiation (W m^{-2}), (c) barometric pressure (mbar), (d) air temperature (°C), (e) water temperature (°C), (f) air-sea temperature difference (°C), (g) relative humidity (%), (h) ΔpCO_2 (ppm), (i) bulk and surface aqueous CO_2 concentrations (μmol L^{-1}), and (j) diurnal variation of atmospheric xCO_2 profiles ensemble-averaged to fractional day. All properties show a coherent trend as a result of the diurnal forcing. The vertical line in each panel indicates the standard deviation. The factional day is in GMT with local time being approximately GMT − 0.3 (≈7 hours).

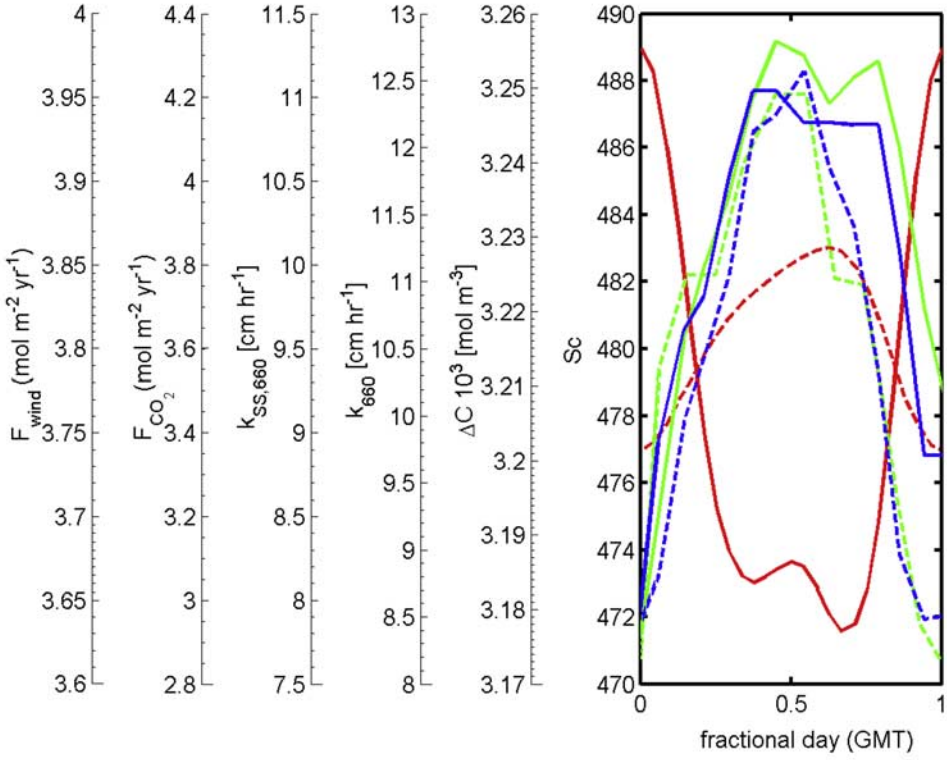

Figure 14. Diurnal ensemble-averaged values of Schmidt number *Sc* (dashed red line), bulk surface aqueous CO_2 difference ΔC (mol m^{-3}) (red line), measured gas transfer velocity k_{660} (cm hr^{-1}) (green line), *Soloviev and Schlüssel* [1994] modeled gas transfer velocity $k_{SS,660}$ (cm hr^{-1}) (dashed green line); measured air-sea CO_2 flux F_{CO2} (mol m^{-2} yr^{-1}) (blue line), and the air-sea CO_2 flux F_{wind} (mol m^{-2} yr^{-1}) based on wind speed correlation (dashed blue line). The diurnal variability of the bulk surface aqueous CO_2 difference is caused by temperature, pressure, and biological effects. The diurnal effect on *Sc* is caused by changes in the surface temperature. The marked increase in nighttime fluxes is >1.2 mol m^{-2} yr^{-1}, representing a 40% increase. A 10% increase in the nighttime CO_2 fluxes is due to wind speed alone.

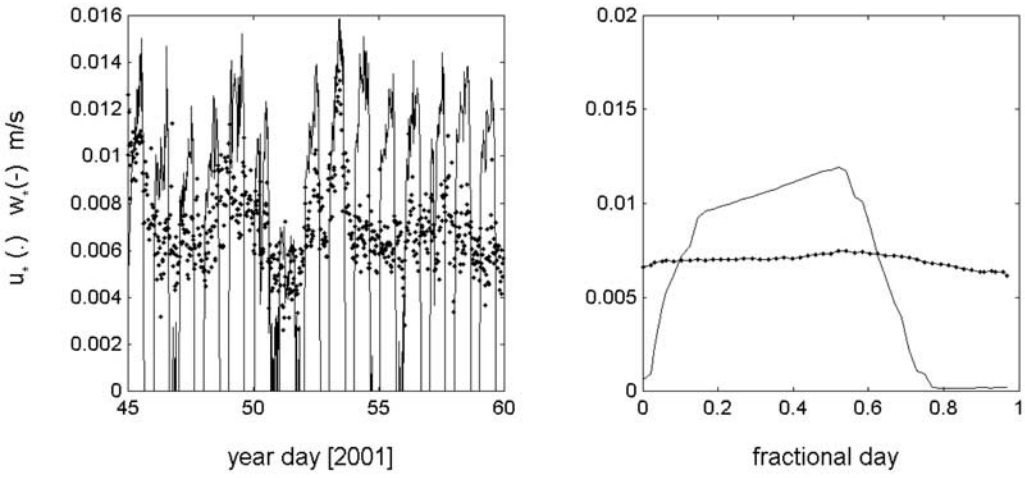

Figure 15. (left) Time series of the characteristic scaling velocities for GasEx-2001 including $u_* = (\tau/\rho)^{1/2}$ and $w_* = (Bh)^{1/3}$. (right) The ensemble average of u_* (solid circle) and w_* (solid line) are shown for fractional day. The buoyancy velocity w_* is large during nighttime cooling and falls off during daytime heating.

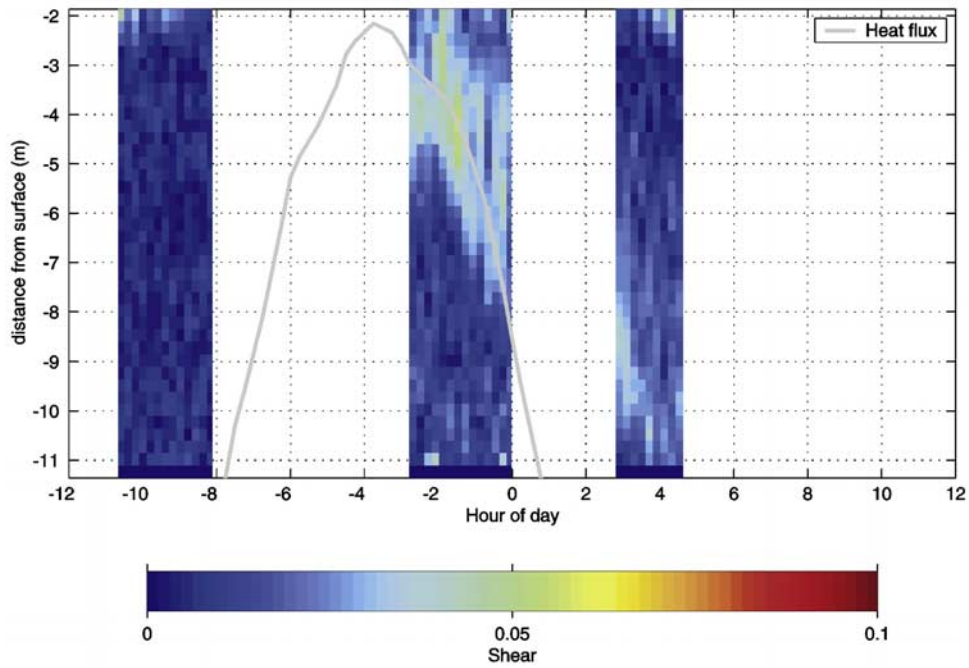

Figure 16. Net heat flux and surface ocean shear measurements made from SPIP. Shear is eroded during nighttime cooling and generated during daytime heating.

layer depth. Equation (17) provides an approximation to the heating in the diurnal mixed layer contributing to energy dissipation. Figure 15 shows the time series and average diurnal cycle of u_* and w_*. The convective velocity scale providing mixing in the surface layer can be as high as the friction velocity scale. Convective velocity scaling has recently been applied to examine the diurnal influence on gas exchange [*MacIntyre et al.*, 2002; *Eugster et al.*, 2003]. This process is particularly relevant for GasEx-2001 because of the persistent diurnal cycle with strong solar heating (>800 W m^{-2}) and moderate wind stress (<0.15 N m^{-2}) resulting in the development of a diurnal mixed layer [*Price et al.*, 1986]. During the day when the surface stratifies, shear is generated near the surface (Figure 16). The momentum balance of the surface layer [*Spigel and Imberger*, 1980] can be approximated by

$$\frac{d(uh)}{dt} = u_*^2. \tag{18}$$

As the diurnal mixed layer depth h is reduced in the daytime, the horizontal surface velocity u increases. Under a water friction velocity of 0.0067 m s^{-1}, typical during GasEx-2001, the surface velocity would increase by more than 20 cm s^{-1} during a 4-hr solar heating cycle. As the mixed layer depth increases and stratification erodes in the afternoon, u decelerates and the surface buoyancy flux increases. These processes, coupled with momentum at the ocean surface, may enhance mixing at night and at the surface during the day. During the night, the surface stress imparted by the wind is transported through the deepening mixed layer. During daytime heating, however, the upper ocean stratifies, and the momentum is confined in a surface layer less than 3 m. This may cause enhanced mixing and surface turbulence throughout the diurnal cycle, resulting in the enhanced gas exchange.

[41] CO_2 exchange at the GasEx-2001 equatorial Pacific study site appears to be forced by thermally induced mixing rather than solely by low winds. However, the magnitude of the measured fluxes was within a factor of 2 of bulk parameterizations [*Feely et al.*, this volume] since the measured fluxes and the parameterizations converge in the 6–8 m/s wind speed range (Figure 10). These results appear indicative of the unique environmental forcing at the study site, in particular, the lack of surfactants and the strong diurnal mixed layer and suggest that simple parameterizations of gas exchange with wind are insufficient in this region. More inclusive algorithms such as those adapted from momentum and heat flux estimates might be more appropriate [*Hare et al.*, 2004]. The process study results show that equatorial Pacific CO_2 exchange is modulated by short-term diurnal cycles in addition to previously reported ENSO cycles.

6. Conclusions

[42] During YD 45–60, the GasEx-2001 process study took place in the South Equatorial Current in the eastern equatorial Pacific at 125°–132°W, 2°–3°S. A combination of ships, buoys, and drifters equipped with state-of-the-art ocean and atmospheric sensors was deployed to measure and assess the variability and surface mechanisms controlling air-sea fluxes with unsurpassed detail. Direct covariance and profile air-sea CO_2 fluxes were measured together with the surface ocean and marine boundary layer processes to obtain a process level mechanistic understanding of gas exchange in the region. The high air-sea pCO_2 difference of 118 μatm provides a high mean transfer of CO_2 to the atmosphere. The study site exhibited high diurnal variations in temperature, chemical and biological activity, and CO_2 flux.

[43] The mean wind speed was 6.0 ± 1.3 m s^{-1}. The mean ocean surface temperature was greater than the air temperature and the atmospheric boundary layer was continually unstable facilitating interpretation of the micrometeorological flux measurements. Diurnal heat fluxes generated daytime upper ocean stratification and strong nighttime buoyancy fluxes. On average, the CO_2 flux from the ocean to the atmosphere was 3.9 mol m^{-2} yr^{-1} with nighttime increases as high as 40%. This is the first time such a diurnal CO_2 flux enhancement was observed over the ocean because the measurement technology used was not previously available.

[44] The GasEx-2001 results show evidence of the air-sea CO_2 exchange with mean values higher than most other predictions at low wind speeds. The high values of CO_2 exchange measured during GasEx-2001 may be attributed to predominantly strong surface turbulent energy driven by diurnal stratification; with possible contributions made by a dearth of surface films, chemical enhancements, and persistence in wind and wave activity.

[45] The 15 days of air-sea flux measurements taken during GasEx-2001 demonstrate some of the systematic environmental trends of the eastern equatorial Pacific Ocean. The fact that local physical processes, in addition to wind, may control the rate of CO_2 transfer from the ocean to the atmosphere indicates that local and global biogeochemical models may need to take local processes into account. These local processes can vary on regional and global scales and suggest that regional parameterizations may be necessary to constrain global air-sea CO_2 fluxes. Our GasEx-2001 results show strong variability in processes governed by the diurnal heating cycle. This implies that any changes in the incident radiation, including atmospheric cloud dynamics, phytoplankton biomass, and surface ocean stratification may have significant feedbacks on the amount and variability of air-sea gas exchange.

[46] **Acknowledgments.** This work was performed with the support of the National Science Foundation Grant OCE-9986724 and the NOAA Global Carbon Cycle Program Grants NA06GP048, NA17RJ1223, and NA87RJ0445 in the Office of Global Programs. The authors wish to thank the crew and captain of the NOAA R/V *Ronald H. Brown* for their outstanding efforts. The authors also wish to express their gratitude for the JGR Editors and anonymous reviewers for increasing the quality and clarity of this manuscript.

References

Asher, W., and R. Wanninkhof (1998), Transient tracers and air-sea gas transfer, *J. Geophys. Res.*, *103*, 15,939–15,958.

Bock, E. J., T. Hara, N. M. Frew, and W. R. McGillis (1999), Relationship between air-sea gas transfer and short wind waves, *J. Geophys. Res.*, *104*, 25,821–25,831.

Bradley, E. F., P. A. Coppin, and J. S. Godfrey (1991), Measurements of sensible and latent heat flux in the western equatorial Pacific Ocean, *J. Geophys. Res.*, *96*, 3375–3389.

Broecker, W. S., and T.-H. Peng (1974), Gas exchange rates between air and sea, *Tellus*, *24*, 21–35.

Broecker, W. S., J. R. Ledwell, T. Takahashi, L. M. R. Weiss, L. Memery, T.-H. Peng, B. Jähne, and K. O. Münnich (1986), Isotopic versus micrometeorological ocean CO_2 fluxes: A serious conflict, *J. Geophys. Res.*, *91*, 10,517–10,527.

Businger, J. A. (1997), On the measurement of the transfer of gases across the air-sea interface, *J. Appl. Meteorol.*, *36*, 1113–1115.

Businger, J. A., and A. C. Delaney (1990), Chemical sensor resolution required for measuring surface fluxes by three common micrometeorological techniques, *J. Atmos. Chem.*, *19*, 399–410.

Coale, K. H., et al. (1996), A massive phytoplankton bloom induced by an ecosystem-scale iron fertilization experiment in the equatorial Pacific Ocean, *Nature*, *383*, 495–501.

Conway, T. J., P. P. Tans, L. S. Waterman, K. W. Thoning, D. R. Kitzis, K. A. Masarie, and N. Zhang (1994), Evidence for interannual variability of the carbon cycle from the NOAA/CMDL global air sampling network, *J. Geophys. Res.*, *99*, 2831–2855.

Dacey, J. W. H., J. B. Edson, P. H. Holland, and W. R. McGillis (1999), In situ estimation of air-sea gas transfer using DMS, paper presented at 13th Symposium on Boundary Layers and Turbulence, Am. Meteorol. Soc., Dallas, Tex.

DeGrandpre, M. D., R. Wanninkhof, W. R. McGillis, and P. G. Strutton (2004), A Lagrangian study of surface pCO_2 dynamics in the eastern equatorial Pacific Ocean, *J. Geophys. Res.*, *109*, C08S07, doi:10.1029/2003JC002089.

Donelan, M. A., and W. M. Drennan (1995), Direct field measurements of the flux of carbon dioxide, in *Air-Water Gas Transfer*, edited by B. Jähneand E. C. Monahan, pp. 677–683, Aeon, Hanau, Germany.

Drennan, W. M., K. K. Kahma, and M. A. Donelan (1999), On momentum flux and velocity spectra over waves, *Boundarey Layer Meteorol.*, *92*, 489–515.

Dyer, A. J. (1974), A review of flux-profile relationships, *Boundarey Layer Meteorol.*, *7*, 363–372.

Edson, J. B., A. A. Hinton, K. E. Prada, J. E. Hare, and C. W. Fairall (1998), Direct covariance flux estimates from mobile platforms at sea, *J. Atmos. Oceanic Technol.*, *15*, 547–562.

Edson, J., C. J. Zappa, J. Ware, W. McGillis, and J. E. Hare (2004), Scalar flux profile relationships over the open ocean, *J. Geophys. Res.*, *109*, C08S09, doi:10.1029/2003JC001960.

Eugster, W., G. Kling, T. Jonas, J. P. McFadden, A. Wüest, S. MacIntyre, and F. S. Chapin III (2003), CO_2 exchange between air and water in an Arctic Alaskan and midlatitude Swiss lake: Importance of convective mixing, *J. Geophys. Res.*, *108*(D12), 4362, doi:10.1029/2002JD002653.

Fairall, C. W., E. F. Bradley, J. S. Godfrey, G. A. Wick, J. B. Edson, and G. S. Young (1996a), Cool-skin and warm-layer effects on sea surface temperature, *J. Geophys. Res.*, *101*, 1295–1309.

Fairall, C. W., E. F. Bradley, D. P. Rogers, J. B. Edson, and G. S. Young (1996b), Bulk parameterization of air-sea fluxes for TOGA-COARE, *J. Geophys. Res.*, *101*, 3747–3764.

Fairall, C. W., J. E. Hare, J. B. Edson, and W. McGillis (2000), Parameterization and micrometeorological measurements of air-sea gas transfer, *Boundary Layer Meteorol.*, *96*, 63–105.

Feely, R. A., R. Wanninkhof, T. Takahashi, and P. Tans (1999), Influence of El Niño on the equatorial Pacific contribution of atmospheric CO_2 accumulation, *Nature*, *398*, 597–601.

Feely, R. A., et al. (2002), Seasonal and interannual variability of CO_2 in the equatorial Pacific, *Deep Sea Res.*, *Part II*, *49*, 2443–2469.

Feely, R. A., R. Wanninkhof, W. McGillis, M.-E. Carr, and C. E. Cosca (2004), Effects of wind speed and gas exchange parameterizations on the air-sea CO_2 fluxes in the equatorial Pacific Ocean, *J. Geophys. Res.*, *109*, C08S03, doi:10.1029/2003JC001896.

Frew, N. M. (1997), The role of organics films in air-sea gas exchange, in *The Sea Surface and Global Change*, edited by R. Duce and P. Liss, pp. 121–172, Cambridge Univ. Press, New York.

Frew, N. M., et al. (2004), Air-sea gas transfer: Its dependence on wind stress, small-scale roughness, and surface films, *J. Geophys. Res.*, *109*, C08S17, doi:10.1029/2003JC002131, in press.

Garbe, C. S., U. Schimpf, and B. Jähne (2004), A surface renewal model to analyze infrared image sequences of the ocean surface for the study of air-sea heat and gas exchange, *J. Geophys. Res.*, *109*, C08S15, doi:10.1029/2003JC001802.

Hare, J. E., C. W. Fairall, W. R. McGillis, J. B. Edson, B. Ward, and R. Wanninkhof (2004), Evaluation of the National Oceanic and Atmospheric Administration/Coupled-Ocean Atmospheric Response Experiment (NOAA/COARE) air-sea gas transfer parameterization using GasEx data, *J. Geophys. Res.*, *109*, C08S11, doi:10.1029/2003JC001831.

Hood, E. M., R. Wanninkhof, and L. Merlivat (2001), Short timescale variations of fCO_2 in a North Atlantic warm-core eddy: Results from the Gas-Ex 98 carbon interface ocean atmosphere (CARIOCA) buoy data, *J. Geophys. Res.*, *106*, 2561–2572.

Imberger, J. (1985), The diurnal mixed layer, *Limnol. Oceanogr.*, *30*, 737–770.

Jacobs, C. M. J., W. Kohsiek, and W. A. Oost (1999), Air-sea fluxes and transfer velocity of CO_2 over the North Sea: Results from ASGAMAGE, *Tellus*, *51*, 629–641.

Jähne, B., and H. Haussecker (1998), Air-water gas exchange, *Annu. Rev. Fluid Mech.*, *30*, 443–468.

Jähne, B., K. O. Münnich, R. Bösinger, A. Dutzi, W. Huber, and P. Libner (1987), On the parameters influencing air-water gas exchange, *J. Geophys. Res.*, *92*, 1937–1949.

Johnson, G. C., C. L. Sabine, K. E. McTaggart, and J. M. Hummon (2004), Physical oceanographic conditions during GasEx 2001, *J. Geophys. Res.*, *109*, C08S04, doi:10.1029/2002JC001718.

Kantha, L. H., and C. A. Clayson (1994), An improved mixed layer model for geophysical applications, *J. Geophys. Res.*, *99*, 25,235–25,266.

Kondo, J. (1975), Air-sea bulk transfer coefficients in diabatic conditions, *Boundary Layer Meteorol.*, *9*, 91–112.

Liss, P. S., and L. Merlivat (1986), Air-sea gas exchange rates: Introduction and synthesis, in *The Role of Air-Sea Exchange in Geochemical Cycles*, edited by P. Buat-Manard, pp. 113–127, D. Reidel, Norwell, Mass.

Liss, P. S., and P. G. Slater (1974), Flux of gases across the air-sea interface, *Nature*, *247*, 181–184.

MacIntyre, S., W. Eugster, and G. W. Kling (2002), The critical importance of buoyancy flux for gas flux across the air-water interface, in *Gas Transfer at Water Surfaces*, *Geophys. Monogr. Ser.*, vol. 127, edited by M. A. Donelan et al., pp. 135–139, AGU.

McGillis, W. R., J. W. H. Dacey, N. M. Frew, E. J. Bock, and B. K. Nelson (2000), Water-air flux of dimethylsulfide, *J. Geophys. Res.*, *105*, 1187–1193.

McGillis, W. R., J. B. Edson, J. E. Hare, and C. W. Fairall (2001a), Direct covariance air-sea CO_2 fluxes, *J. Geophys. Res.*, *106*, 16,729–16,745.

McGillis, W. R., J. B. Edson, J. D. Ware, J. W. H. Dacey, J. E. Hare, C. W. Fairall, and R. Wanninkhof (2001b), Carbon dioxide flux techniques performed during GasEx-98, *Mar. Chem.*, *75*, 267–280.

McKenna, S. P., and W. R. McGillis (2004), The role of free-surface turbulence and surfactants in air-water gas transfer, *Int. J. Heat Mass Transfer*, *47*, 539–553.

McNeil, C. L., and L. Merlivat (1996), The warm oceanic surface layer: Implications for CO_2 fluxes and surface gas measurements, *Geophys. Res. Lett.*, *23*, 3575–3578.

Merlivat, L., and P. Brault (1995), CARIOCA buoy: Carbon dioxide monitor, *Sea Technol.*, *10*, 23–30.

Mitchell, G. M. (2001), Determination of vertical fluxes of sulfur dioxide and dimethyl sulfide in the remote marine atmosphere by eddy correlation and an airborne isotopic dilution atmospheric pressure ionization mass spectrometer, Ph.D. thesis, 234 pp., Drexel Univ., Philadelphia, Pa.

Nightingale, P. N., P. S. Liss, and P. Schlosser (2000), Measurement of air-sea gas transfer during an open ocean algal bloom, *Geophys. Res. Lett.*, *27*, 2117–2120.

Panofsky, H. A., and J. A. Dutton (1984), *Atmospheric Turbulence*, Wiley-Interscience, Hoboken, N.J.

Paulson, C. A. (1970), The mathematical representation of wind speed and temperature profiles in the unstable atmospheric surface layer, *J. Appl. Meteorol.*, *9*, 857–861.

Peng, T.-H., T. Takahashi, W. S. Broecker, and J. Olafsson (1987), Seasonal variability of carbon dioxide, nutrients and oxygen in the northern North Atlantic surface water: Observations and a model, *Tellus*, *Ser. B, 39*, 439–458.

Price, J. F., R. A. Weller, and R. Pinkel (1986), Diurnal cycling: Observations and model of the upper ocean response to diurnal heating, cooling and wind mixing, *J. Geophys. Res.*, *91*, 8411–8427.

Robertson, J. E., and A. J. Watson (1992), Thermal skin effect of the surface ocean and its implication for CO_2 uptake, *Nature*, *358*, 738–740.

Sabine, L. C., R. A. Feely, G. C. Johnson, P. G. Strutton, M. F. Lamb, and K. E. McTaggart (2004), A mixed layer carbon budget for the GasEx-2001 experiment, *J. Geophys. Res.*, *109*, C08S05, doi:10.1029/2002JC001747.

Schimpf, U., C. Garbe, and B. Jähne (2004), Investigation of transport processes across the sea-surface microlayer by infrared imagery, *J. Geophys. Res.*, *109*, C08S13, doi:10.1029/2003JC001803.

Schlüssel, P., W. J. Emery, H. Grassl, and T. Mammen (1990), On the bulk-skin temperature difference and its impact on satellite remote sensing measurements of sea surface temperature, *J. Geophys. Res.*, *95*, 13,341–13,356.

Siegel, D. A., S. Maritorena, N. B. Nelson, D. A. Hansell, and M. Lorenzi-Kayser (2002), Global distribution and dynamics of colored dissolved and detrital organic materials, *J. Geophys. Res.*, *107*(C12), 3228, doi:10.1029/2001JC000965.

Smith, S. D., and E. P. Jones (1985), Evidence for wind-pumping of air-sea exchange based on direct measurements of CO_2 fluxes, *J. Geophys. Res.*, *90*, 869–875.

Soloviev, A. V., and P. Schlüssel (1994), Parameterization of the cool skin of the ocean and of the air-ocean gas transfer on the basis of modeling surface renewal, *J. Phys. Oceanogr.*, *24*, 1339–1346.

Spigel, R. H., and J. Imberger (1980), The classification of mixed layer dynamics in lakes of small to medium size, *J. Phys. Oceanogr.*, *10*, 1104–1121.

Strutton, P. G., F. P. Chavez, R. C. Dugdale, and V. Hogue (2004), Primary productivity in the central equatorial Pacific (3°S 130°W) during GasEx-2001, *J. Geophys. Res.*, *109*, C08S06, doi:10.1029/2003JC001790.

Takahashi, T., J. Olafsson, J. G. Goddard, D. W. Chipman, and S. C. Sutherland (1993), Seasonal variations of CO_2 and nutrients in the high-latitude surface oceans: A comparative study, *Global Biogeochem. Cycles*, *7*, 843–878.

Van Scoy, K. A., K. P. Morris, J. E. Robertson, and A. J. Watson (1995), Thermal skin effect and the air-sea flux of carbon dioxide: A seasonal high-resolution estimate, *Global Biogeochem. Cycles*, *9*, 253–262.

Wanninkhof, R. (1992), Relationship between wind speed and gas exchange over the ocean, *J. Geophys. Res.*, *97*, 7373–7382.

Wanninkhof, R., and M. Knox (1996), Chemical enhancement of CO_2 exchange in natural waters, *Limnol. Oceanogr.*, *41*, 689–698.

Wanninkhof, R., and W. R. McGillis (1999), A cubic relationship between air-sea CO_2 exchange and wind speed, *Geophys. Res. Lett.*, *26*, 1889–1892.

Wanninkhof, R., and K. Thoning (1993), Measurement of fugacity of CO_2 in surface water using continuous and discrete sampling methods, *Mar. Chem.*, *44*, 189–204.

Wanninkhof, R., K. F. Sullivan, and Z. Top (2004), Air-sea gas transfer in the Southern Ocean, *J. Geophys. Res.*, *109*, C08S19, doi:10.1029/2003JC001767.

Ward, B., R. Wanninkhof, W. R. McGillis, A. T. Jessup, M. D. DeGrandpre, J. E. Hare, and J. B. Edson (2004), Biases in the air-sea flux of CO_2 resulting from ocean surface temperature gradients, *J. Geophys. Res.*, *109*, C08S08, doi:10.1029/2003JC001800.

Webb, E. K., G. I. Pearman, and R. Leuning (1980), Correction of flux measurements for density effects due to heat and water vapour transfer, *Q. J. R. Meteorol. Soc.*, *106*, 85–100.

Weiss, R. F. (1974), Carbon dioxide in water and seawater: The solubility of a nonideal gas, *Mar. Chem.*, *2*, 203–215.

Zemmelink, H. J., J. W. H. Dacey, E. J. Hintsa, W. R. McGillis, W. W. C. Gieskes, W. Klaassen, H. W. de Groot, and H. J. W. de Baar (2004), Fluxes and gas transfer rates of the biogenic trace gas DMS derived from atmospheric gradients, *J. Geophys. Res.*, *109*, C08S10, doi:10.1029/2003JC001795.

Zhang, J.-Z., R. Wanninkhof, and K. Lee (2001), Enhanced new production observed from the diurnal cycle of nitrate in an oligotrophic anticyclonic eddy, *Geophys. Res. Lett.*, *28*, 1579–1582.

M. D. DeGrandpre, Department of Chemistry, University of Montana, Missoula, MT 59812, USA.

M. Donelan and W. Drennan, Division of Applied Marine Physics, Rosenstiel School of Marine and Atmospheric Science, University of Miami, 4600 Rickenbacker Causeway, Miami, FL 33149-1098, USA.

J. B. Edson, S. P. McKenna, E. A. Terray, and J. D. Ware, Department of Applied Ocean Physics and Engineering, Woods Hole Oceanographic Institution, MS #11, Woods Hole, MA 02543, USA.

C. W. Fairall, NOAA Environmental Technology Laboratory, 325 Broadway, Boulder, CO 80305, USA.

R. A. Feely, Pacific Marine Environmental Laboratory, National Oceanic and Atmospheric Administration, Bin C15700, 7600 Sand Point Way NE, Seattle, WA 98115, USA.

J. E. Hare, Cooperative Institute for Research in Environmental Sciences, University of Colorado, Campus Box 216, Boulder, CO 80309, USA.

W. R. McGillis and C. J. Zappa, Lamont-Doherty Earth Observatory, Palisades, NY 10964, USA. (wrm2102@columbia.edu)

R. Wanninkhof, Atlantic Oceanographic and Meteorological Laboratory, National Oceanic and Atmospheric Administration, 4301 Rickenbacker Causeway, Miami, FL 33149, USA.